Chapter 3

Ratcheting Fatigue Behaviour of Modified 9Cr-1Mo steel at RT

3.1 Introduction

This chapter presents microstructure, tensile properties, and uniaxial ratcheting fatigue behaviour of the modified 9Cr-1Mo steel in normalized and tempered condition, at room temperature. A detailed study was carried out on uniaxial ratcheting fatigue behaviour using various parameters such as mean stress (190-210 MPa); stress amplitude (400-420 MPa) and stress rate (50-450 MPa/s), using 50 kN servo-hydraulic MTS fatigue testing machine. The test matrix of ratcheting fatigue at various parameters was prepared, based on the tensile test data at a strain rate of $10^{-3}s^{-1}$, at room temperature. The test matrix was prepared in such a way that the maximum stress was above the yield strength of the material. While studying the effect of one parameter, the other parameters were kept constant.

Cyclic hardening/ softening or cyclic stability of the material, under asymmetric loading, is depicted with the aid of cyclic stress-strain hysteresis loops, corresponding to different number of cycles. The tests were conducted till fracture and the fractographic analysis of the fractured specimens was done using scanning electron microscopy and deformation behaviour along with dislocation substructure developed during the asymmetrical loading was characterized by transmission electron microscopy.

3.2 Microstructural characterization of modified 9Cr-1Mo steel

The microstructure of the modified 9Cr-1Mo steel in the normalized and tempered condition shows lath martensite with second phase particles under optical and scanning electron microscope as shown in Fig. 3.1. The optical micrograph shows microstructure with prior austenite grain boundaries (PAGbs) (Fig. 3.1a). These grain boundaries decorated with carbide precipitates are revealed more clearly in the SEM micrograph (Fig. 3.1b)

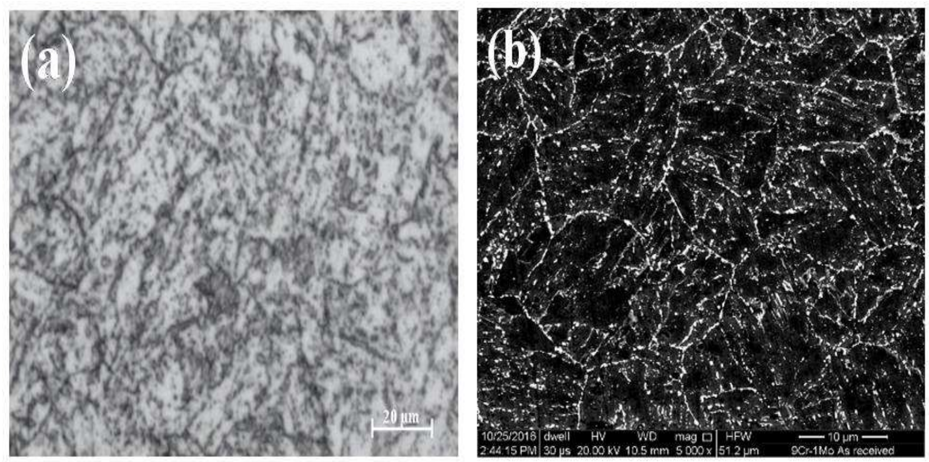

Fig. 3.1 Microstructure of the modified 9Cr-1Mo steel in normalized and tempered condition: (a) optical micrograph showing lath martensitic structure and (b) SEM micrograph depicting precipitates along grain boundaries.

Second phase particles along the PAGbs and lath boundaries are evident from the TEM micrograph (Fig. 3.2a). Also, there are fine second phase particles within the laths. In addition to second phase precipitates along the martensite lath boundaries, high density of dislocations may be seen within the laths (Fig. 3.2b). There are different morphologies of the second phase particles. Crystal structures of the matrix and precipitates were analyzed from their selected area diffraction (SAD) patterns. Crystal structure of the matrix and precipitates are characterized as *bcc* and *fcc* respectively (Fig. 3.2c).

Lattice parameters of the different types of precipitates were calculated from their SAD patterns and compared with the JCPDS. The cuboidal particles are identified as $Cr_{23}C_6$ carbide with lattice parameter *a*: 10.65 Å. In addition to these, round precipitates of niobium carbide (NbC) and rod like precipitates of vanadium carbide (VC) are observed which are consistent with the earlier findings in normalized and tempered condition of the present steel [Jones et al., (1991); Paul et al., (2008)].

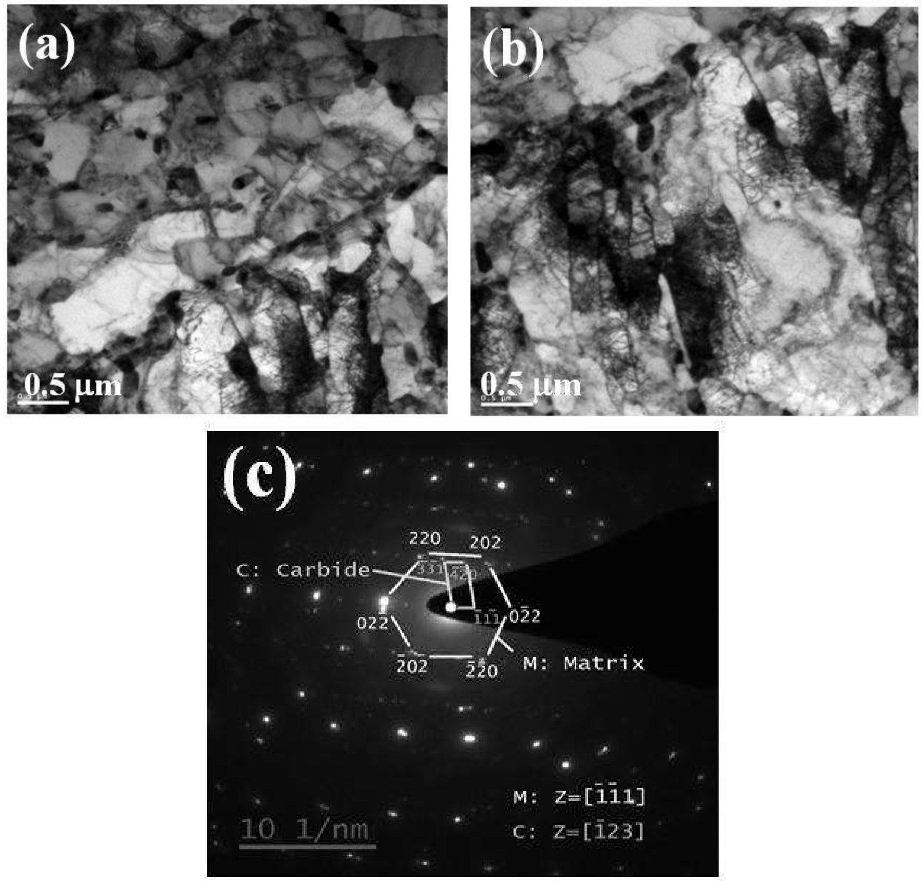

Fig. 3.2 TEM micrographs of modified 9Cr-1Mo steel showing: (a) second phase particles of $M_{23}C_6$ carbides along the prior austenite grain boundaries and fine MX carbides within the laths (b) laths with high density of dislocations and (c) diffraction pattern of the matrix *(bcc)* and $Cr_{23}C_6$ precipitate *(fcc)*.

3.3 Tensile properties of modified 9Cr-1Mo steel

The engineering stress-strain curve of the modified 9Cr-1 Mo steel in the normalized and tempered condition, tested at a strain rate of 10^{-3} s^{-1} is displayed in Fig. 3.3 and the tensile properties are listed in Table 3.1. The test matrix of the ratcheting fatigue was formed based on the values of yield strength and tensile strength. The maximum applied load was taken above the yield strength.

Table 3.1 Strength and ductility parameters of the normalized and tempered modified 9Cr-1Mo steel, tested at strain rate of 10^{-3} s^{-1}, at RT.

0.2% Yield Strength (MPa)	Ultimate Tensile Strength (MPa)	Elongation (%)	Uniform plastic elongation (%)	Reduction in area (%)	Strength coefficient (K) (MPa)	Strain hardening exponent (n)	Degree of work hardening (S_{UTS} /S_{YS})
575	713	26	8	74	933	0.090	1.24

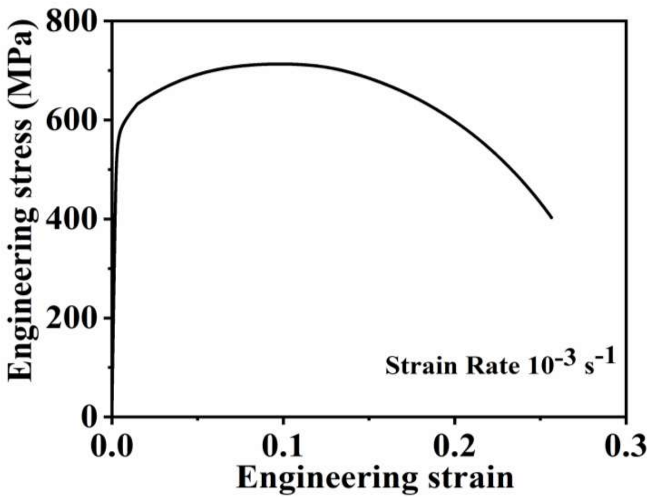

Fig. 3.3 Engineering stress strain curve of the modified 9Cr-Mo steel in normalized and tempered condition, tested at a strain rate of 10^{-3} s^{-1}, at room temperature.

3.4 Uniaxial ratcheting fatigue behaviour of modified 9Cr-1Mo steel

Hysteresis loops of the specimens tested at room temperature under asymmetric cyclic loading with mean stress of 190 MPa, stress amplitude of 410 MPa and stress rate of 150 MPa/s are displayed in Fig. 3.4(a). The applied maximum stress (σ_{max}) and minimum stress (σ_{min}) was 600 MPa and -220 MPa respectively. The hysteresis loops may be noticed to be partially closed in the beginning, as the loading was asymmetric; however, the extent of non-closure continuously decreased with increase in cycles. The shifting of loops towards right side led to progressive increase in the permanent deformation.

There was fast rise in the accumulating ratcheting strain in the beginning, as seen from the enlarged view (Fig. 3.4c), up to about 10 cycles; however, the increase was very slow during the subsequent cycles till about 6000 cycles, after that there was very rapid increase till the fracture (Fig. 3.4b).

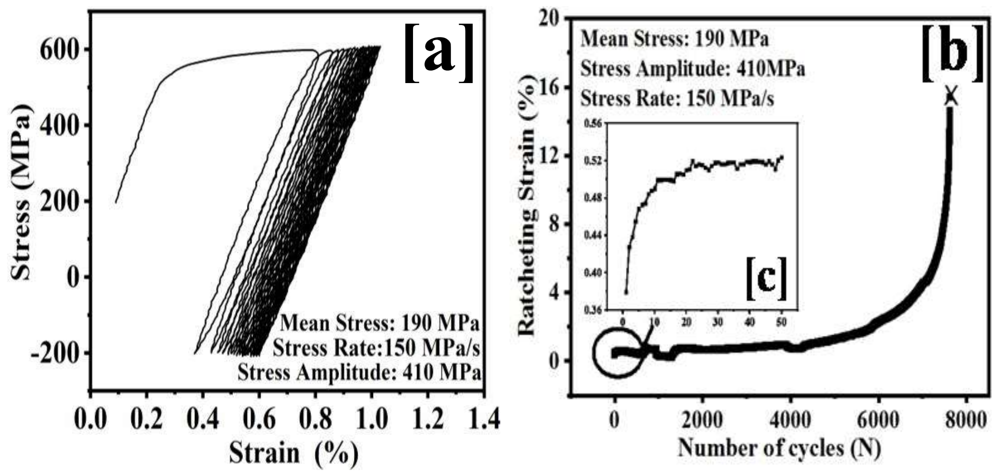

Fig. 3.4 Ratcheting behaviour of modified 9Cr-1Mo steel during asymmetric cyclic loading at room temperature: (a) decrease in loop width with cycles (b) variation of ratcheting strain with cycles during asymmetric cyclic loading and (c) rapid increase in ratcheting strain during the initial 10 cycles, shown on a magnified scale.

3.4.1 Influence of mean stress on fatigue behaviour of modified 9Cr-1Mo steel under asymmetric cyclic loading

For understanding the influence of tensile mean stress on the accumulation of ratcheting strain and fatigue life, fatigue tests were carried out with asymmetric stress cycling at different mean stresses, keeping the stress amplitude and stress rate constant at 400 MPa and 150 MPa/s, respectively. Ratcheting cyclic life is presented in Table 3.2 for mean stress varying from 190 to 210 MPa. It can be seen from Table 3.2 that the number of cycles to failure (N_f) decreased with rise in the mean stress from 190 to 210 MPa.

Table 3.2 Variation of fatigue life of modified 9Cr-1Mo steel, under asymmetric cyclic loading at various mean stresses, tested at stress amplitude of 410 MPa and stress rate of 150 MPa/s.

S.No.	Maximum stress (σ_{max}) MPa	Minimum stress (σ_{min}) MPa	Mean stress (σ_m) MPa	No. of cycles to failure (N_f)
1	600	-220	**190**	7620
2	610	-210	**200**	4411
3	620	-200	**210**	1506

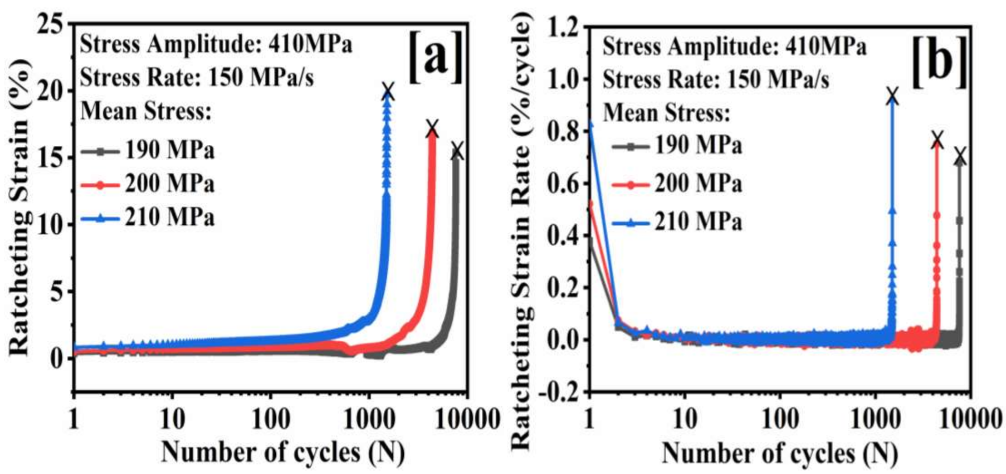

Fig. 3.5 Influence of mean stress on ratcheting behaviour of modified 9Cr-1Mo steel showing: (a) change in ratcheting strain with cycles under different mean stresses and (b) ratcheting strain rate with number of cycles.

Fig. 3.5(a) depicts the change in the accumulating ratcheting strain with cycles up to failure, at varying mean stresses. The results show high rate of accumulation of plastic strain with rise in mean stress from 190 to 210 MPa. The ratcheting rate decreased rapidly during the initial 2/3 cycles, remained nearly constant upto 1000 cycles or more depending on the mean stress, and increased rapidly in the last stage till fracture. The rate of accumulation of ratcheting strain was high at the highest mean stress (Fig. 3.5b).

3.4.2 Influence of stress amplitude on fatigue behaviour of modified 9Cr-1Mo steel under asymmetric cyclic loading

Fatigue tests were performed under asymmetric cyclic loading at various stress amplitudes from 400 to 420 MPa, at a constant mean stress of 200 MPa and stress rate of 150 MPa/s and the results are presented in Table 3.3

Table 3.3 Variation of fatigue life of modified 9Cr-1Mo steel, under asymmetric cyclic loading at various stress amplitudes, tested at mean stress of 200 MPa and stress rate of 150 MPa/s.

S.No.	Maximum stress (σ_{max}) MPa	Minimum stress (σ_{min}) MPa	Stress amplitude (σ_a) MPa	No. of cycles to failure (N_f)
1	600	-200	**400**	16135
2	610	-210	**410**	4411
3	620	-220	**420**	2117

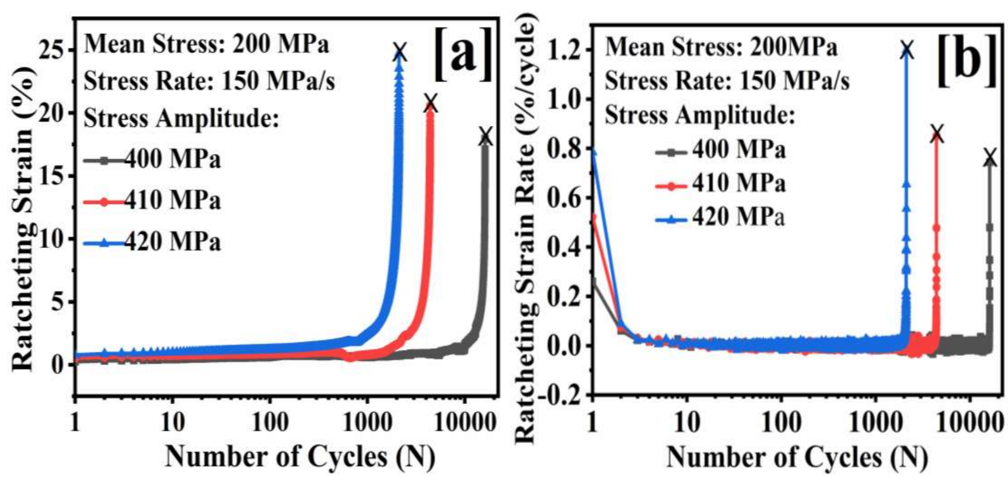

Fig. 3.6 Influence of stress amplitude on ratcheting behaviour of modified 9Cr-1Mo steel showing: (a) change in ratcheting strain with cycles under different stress amplitudes and (b) ratcheting strain rate with number of cycles.

It is evident that with an increase in stress amplitude from 400 to 420 MPa, the cyclic life was reduced. The change in ratcheting strain with number of cycles to failure at varying stress amplitudes is displayed in Fig. 3.6(a). It is observed that with a rise in stress amplitude, the accumulation of ratcheting strain increases, similar to that in the case of mean stress.

Similarly, the rate of accumulation of ratcheting strain was also increased with a rise in the stress amplitude, causing a reduction in fatigue life (Fig. 3.6 b).

3.4.3 Influence of stress rate on fatigue behaviour of modified 9Cr-1Mo steel under asymmetric cyclic loading

Fatigue tests were carried out under asymmetric stress cycling at different stress rates of 50,150 and 450 MPa/s at constant stress amplitude of 410 MPa and tensile mean stress of 200 MPa.

Table 3.4 Variation of fatigue life of modified 9Cr-1Mo steel, under asymmetric cyclic loading at various stress rates, tested at mean stress of 200 MPa and stress amplitude of 410 MPa.

S.No.	Maximum stress (σ_{max}) MPa	Minimum stress (σ_{min}) MPa	Stress rate ($\dot{\sigma}$) MPa/s	No. of cycles to failure (N_f)
1	610	-210	**50**	1783
2	610	-210	**150**	4411
3	610	-210	**450**	6460

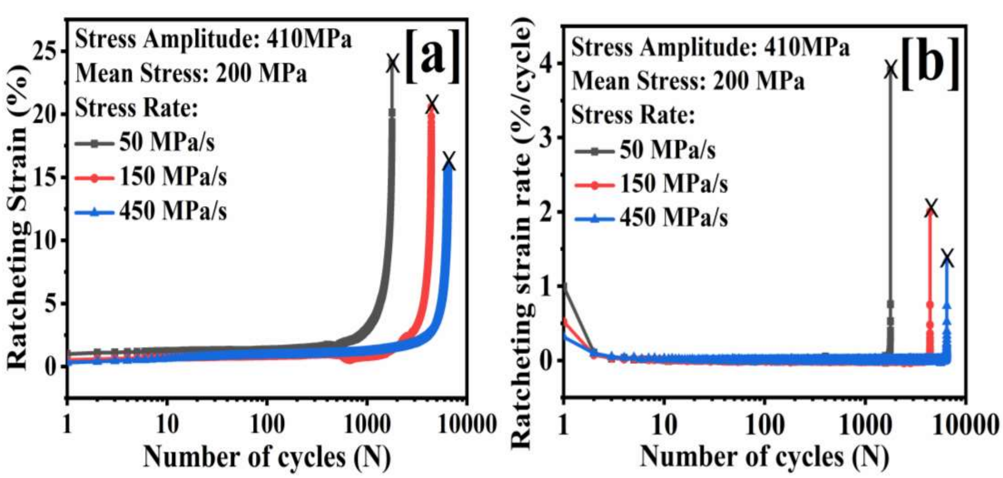

Fig. 3.7 Influence of stress rate on ratcheting fatigue behaviour of modified 9Cr-1Mo steel showing: (a) change in ratcheting strain with cycles at different stress rates and (b) ratcheting strain rate with number of cycles.

It can be observed from Table 3.4 that with an increase in the stress rate from 50 MP/s to 450 MP/s, there is an improvement in ratcheting fatigue life. Fig. 3.7(a) depicts the change in accumulating permanent strain with cyclic loading at varying stress rates. Further, with an increase in stress rate, the rate of accumulation of ratcheting strain is reduced (Fig. 3.7b) and fatigue life is improved.

3.5 Cyclic stress-strain behaviour of modified 9Cr-1Mo steel

Plastic strain accumulates due to asymmetric cyclic loading. A number of researchers have investigated cyclic stress-strain behaviour and found that it depends not only on the material but also on the magnitude of the stress and stress profile. Various studies have shown that stainless steels and pure copper display cyclic hardening, while 1070 steel exhibits cyclic softening. In general, hardened materials (cold worked, quenched) undergo cyclic softening and soft materials (annealed) exhibit cyclic hardening [Paul et al., (2010)]. Based on the width of hysteresis loops, cyclic stress-strain behaviour of the modified 9Cr-1 Mo steel was evaluated, for the various combinations of mean stress, stress amplitude and stress rate.

3.5.1 Impact of mean stress on stress-strain behaviour of modified 9Cr-1Mo steel under asymmetric cyclic stressing

Keeping a particular combination of the three variables, comparison was made of the hysteresis loops in terms of their widths at different number of cycles. In Fig. 3.8, the effect of mean stress from 190 MPa to 210 MPa, at constant stress amplitude of 410 MPa, and stress rate of 150 MPa/s is presented at different number of cycles (5, 50 and 500). The general rule is that more the hysteresis loop area, more is the energy absorbed by the material and lesser is the fatigue life. As shown in Fig. 3.8, at the constant stress amplitude of 410 MPa, the width of hysteresis loops increased with increase in mean stress from 190 to 210 MPa. The increase in the width of loops with rise in mean stress was due to increased plastic deformation of the material.

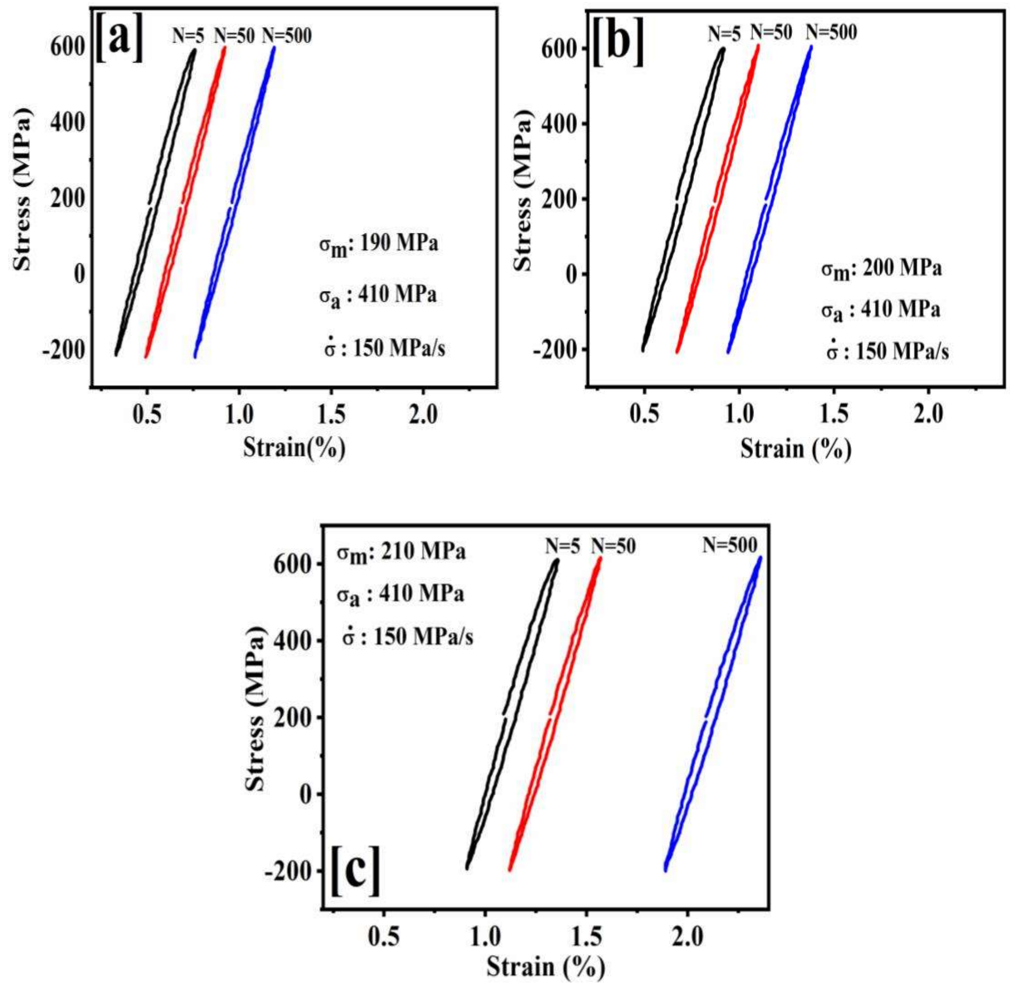

Fig. 3.8 Hysteresis loops of modified 9Cr-1Mo steel corresponding to stress cycle number 5, 50 and 500, at various mean stresses: (a) 190 MPa (b) 200 MPa and (c) 210 MPa, at stress amplitude of 410 MPa and stress rate of 150 MPa/s.

Fig. 3.9 shows variation of the hysteresis loop energy with mean stress. It may be seen that the plastic strain energy per cycle decreases with increase in the number of cycles at all the three levels of mean stress which reflects cyclic hardening of the material with increase in number of cycles. In general, the plastic strain energy increases with increase in mean stress at 5, 50 and 500 cycles. However, at mean stress of 200 and 210 MPa, the plastic strain energy at 500 cycles is higher than that at 50 cycles. This shows that plastic deformation increases at 500 cycles and the effect is more pronounced at the highest mean stress of 210 MPa.

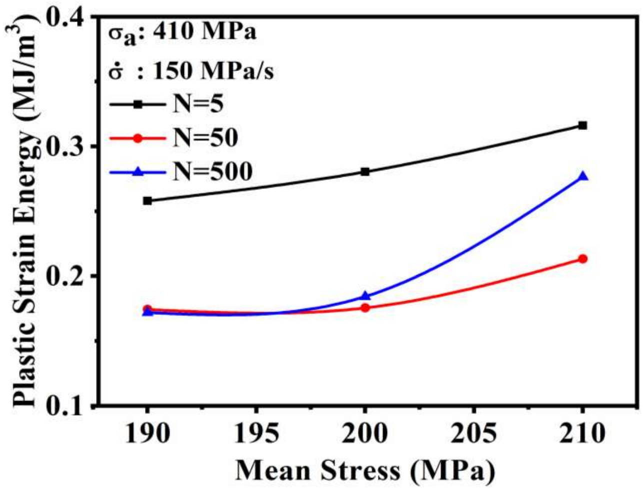

Fig. 3.9 Effect of mean stress on hysteresis loop energy of modified 9Cr-1Mo steel, at different number of cycles, at constant stress amplitude of 410 MPa and stress rate of 150 MPa/s.

Fig. 3.10 shows variation of plastic strain energy with number of cycles till failure at different mean stresses. It is evident from Table 3.5 that at the mean stress of 210 MPa, plastic strain energy in the first cycle was very high (3.92 MJ/m^3) and drastically reduced (0.52 MJ/m^3) in the second cycle. There was continued decrease in the plastic strain energy (Table 3.5) till the 90th cycle (0.21MJ/m^3), however, it started increasing during further cycling and reached 0.27 MJ/m^3 at 500 cycles. Thus, it is obvious that plastic deformation in the first cycle occurred easily; however, cyclic hardening occurred during the subsequent cycles up to the 90th cycle and beyond that there was cyclic softening of the material at slow rate. There is a similar trend in the variation of the plastic strain energy with number of cycles at the mean stress of 190 and 200 MPa also.

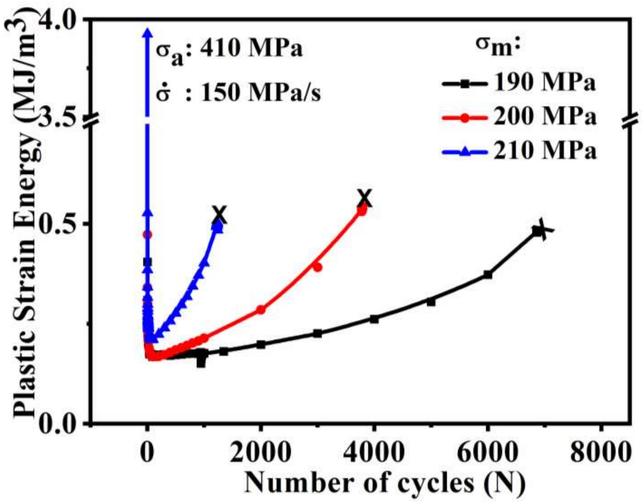

Fig. 3.10 Variation of plastic strain energy with number of cycles, of modified 9Cr-1Mo steel, at different mean stresses, at constant stress amplitude of 410 MPa and stress rate of 150 MPa/s.

Table 3.5 Variation of plastic strain energy of modified 9Cr-1Mo steel, with mean stress and number of cycles.

Cycle Number	Plastic Strain Energy (MJ/m^3)		
	σ_m = 190 MPa	σ_m = 200 MPa	σ_m = 210 MPa
1	1.72	2.23	3.92
2	0.40	0.47	0.52
90	0.16	0.16	0.21
500	0.17	0.18	0.27
1000	0.18	0.21	0.40

From the TEM micrograph in Fig. 3.11(a), second phase particles are observed which are indicated by circles and easy movement of dislocations can be seen resulting in softening. The cyclic hardening after the first cycle resulted from interaction between the dislocations and precipitates of different carbides ($Cr_{23}C_6$, VC, NbC) along the boundaries as indicated by arrows and also due to pinning of dislocations, marked by circles in Fig. 3.11(b). The relatively large extent of cyclic softening during the later stage of cycling, at all the stress amplitudes may be attributed mainly to the substructure, formed by a process of dynamic recovery as shown in Fig. 3.11(c).

These features of the TEM micrographs are similar to those observed earlier by Verma et.al., (2016) in the present steel during symmetrical cyclic loading (R= -1) tested in strain control mode.

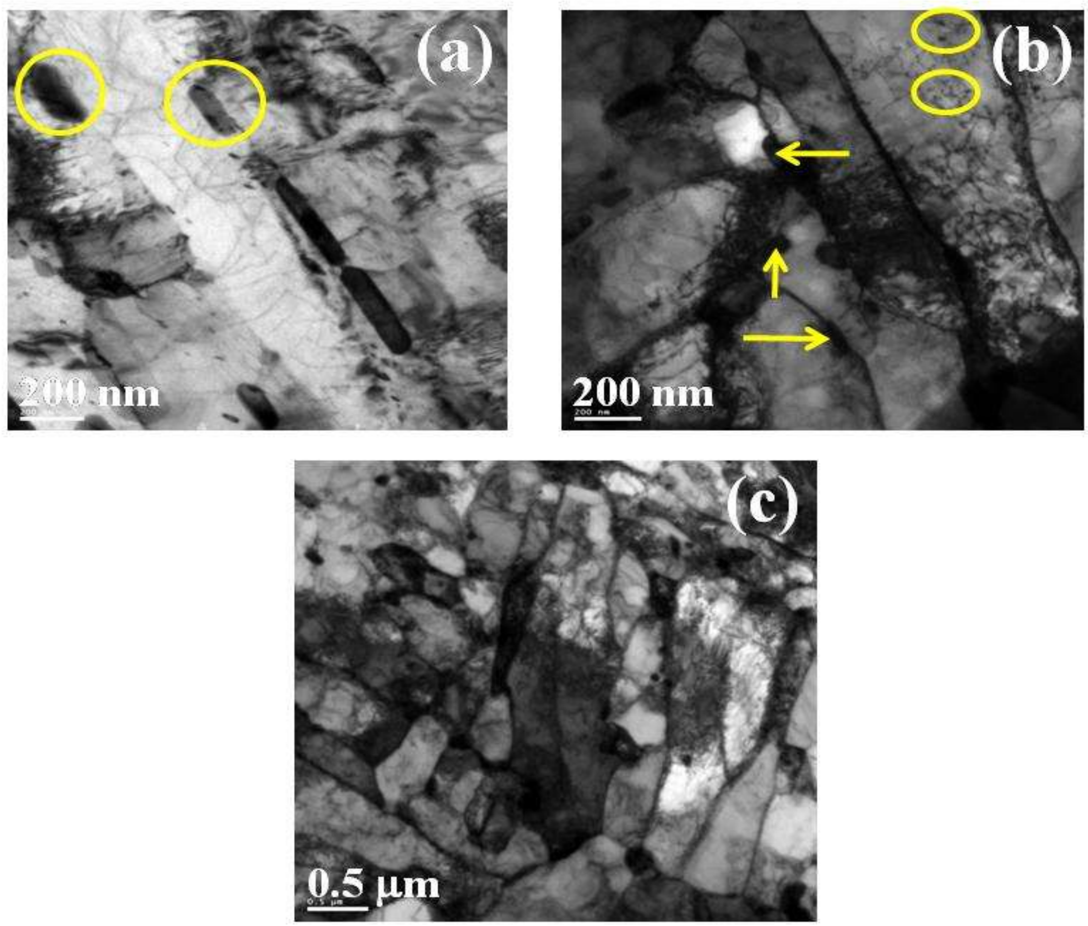

Fig. 3.11 TEM micrographs of the modified 9Cr-1Mo steel in normalized and tempered condition, tested at the mean stress of 210 MPa, stress amplitude of 400 MPa, stress rate of 150 MPa/s showing: (a) easy movement of dislocations, (b) arrows show interaction of dislocations and precipitates whereas circles indicate pinning of dislocations and (c) formation of substructure by a process of dynamic recovery.

3.5.2 Impact of stress amplitude on stress-strain behaviour of modified 9Cr-1Mo steel under asymmetric cyclic stressing

The impact of stress amplitude on hysteresis loops at mean stress of 200 MPa and stress rate of 150 MPa/s is shown in Fig. 3.12.The increase in the width of loops with increase in stress amplitude may be seen to be similar to that observed for the effect of mean stress and this behaviour may be attributed to higher plastic deformation.

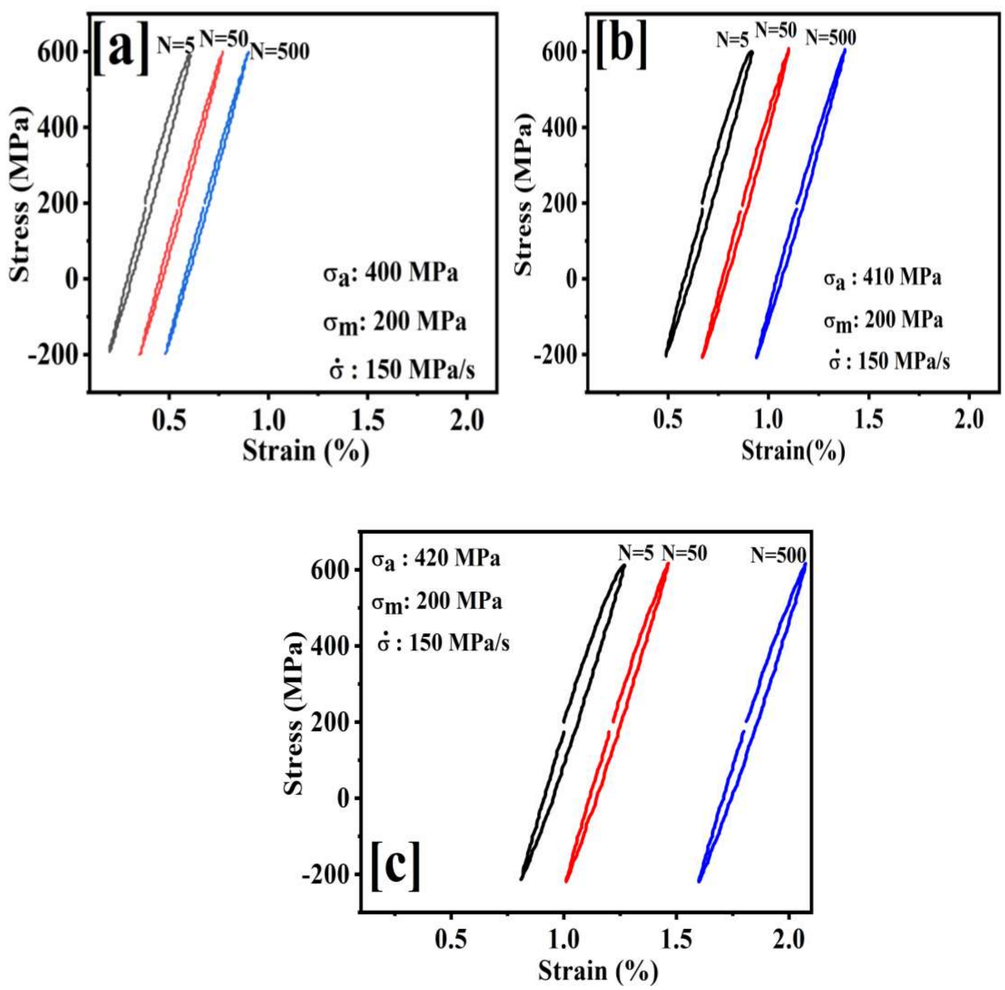

Fig. 3.12 Hysteresis loops of modified 9Cr-1Mo steel corresponding to cycle number 5, 50 and 500 at various stress amplitudes: (a) 400 MPa (b) 410 MPa and (c) 420 MPa, at mean stress of 200 MPa and stress rate of 150 MPa/s.

It may be noticed from Fig. 3.12 that with increase in stress amplitude, the width of loops increases; thus, there is increase in the extent of plastic deformation with increase in this parameter.

Fig. 3.13 shows variation of plastic strain energy with stress amplitude for different number of cycles. The plastic strain energy is the highest in the 5th cycle as compared to those in the 50th and 500th cycles, at all the three levels of stress amplitude. Likewise, there was maximum deformation during the initial stage and was followed by cyclic hardening during the subsequent cycles at all the three levels of stress amplitude.

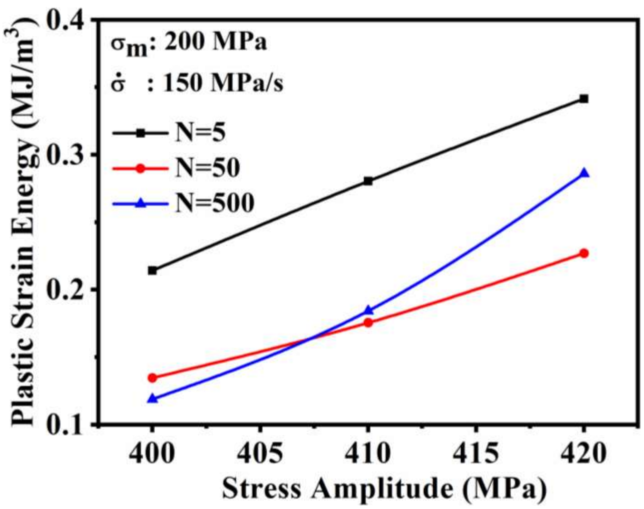

Fig. 3.13 Effect of stress amplitude on hysteresis loop energy of modified 9Cr-1Mo steel, at different number of cycles at constant mean stress of 200 MPa and stress rate of 150 MPa/s.

It is evident from Fig. 3.13 that with increase in stress amplitude, the absorbed plastic strain energy increased due to higher plastic deformation of the material. Fig. 3.14 illustrates variation of plastic strain energy with number of cycles to failure at various stress amplitudes.

The variation of plastic strain energy at different stress amplitudes with number of cycles till failure is shown in Fig. 3.13. The absorbed plastic strain energy increased with increase in stress amplitude, due to increase in accumulation of plastic strain with consequent decrease in fatigue life.

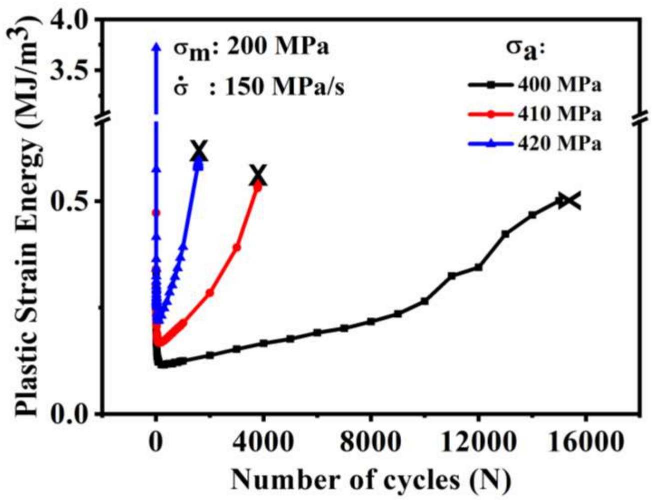

Fig. 3.14 Variation of plastic strain energy with number of cycles of modified 9Cr-1Mo steel, at different stress amplitudes at constant stress of 200 MPa and stress rate of 150 MPa/s.

3.5.3 Impact of stress rate on stress-strain behaviour of modified 9Cr-1Mo steel under asymmetric cyclic stressing

The impact of stress rate on the hysteresis loops at mean stress of 200 MPa and stress amplitude of 410 MPa is shown Fig. 3.15.

It may be observed from Fig.3.15 (a) that at the stress rate of 50 MPa/s, the width of the loop is more at 50^{th} cycle than that at 5^{th} cycle; however, the loop width is decreased at 500^{th} cycle. On the other hand, at the higher stress rate of 150 and 450 MPa/s, the loop width continuously decreased from the 5^{th} to 500^{th} cycle (Fig. 3.15b and c).The width of the loop corresponding to stress rate of 50 MPa/s is larger, than those of the loops corresponding to the stress rate of 150 and 450 MPa/s at 500th cycle. Thus, with increase in the stress rate, hardening increases.

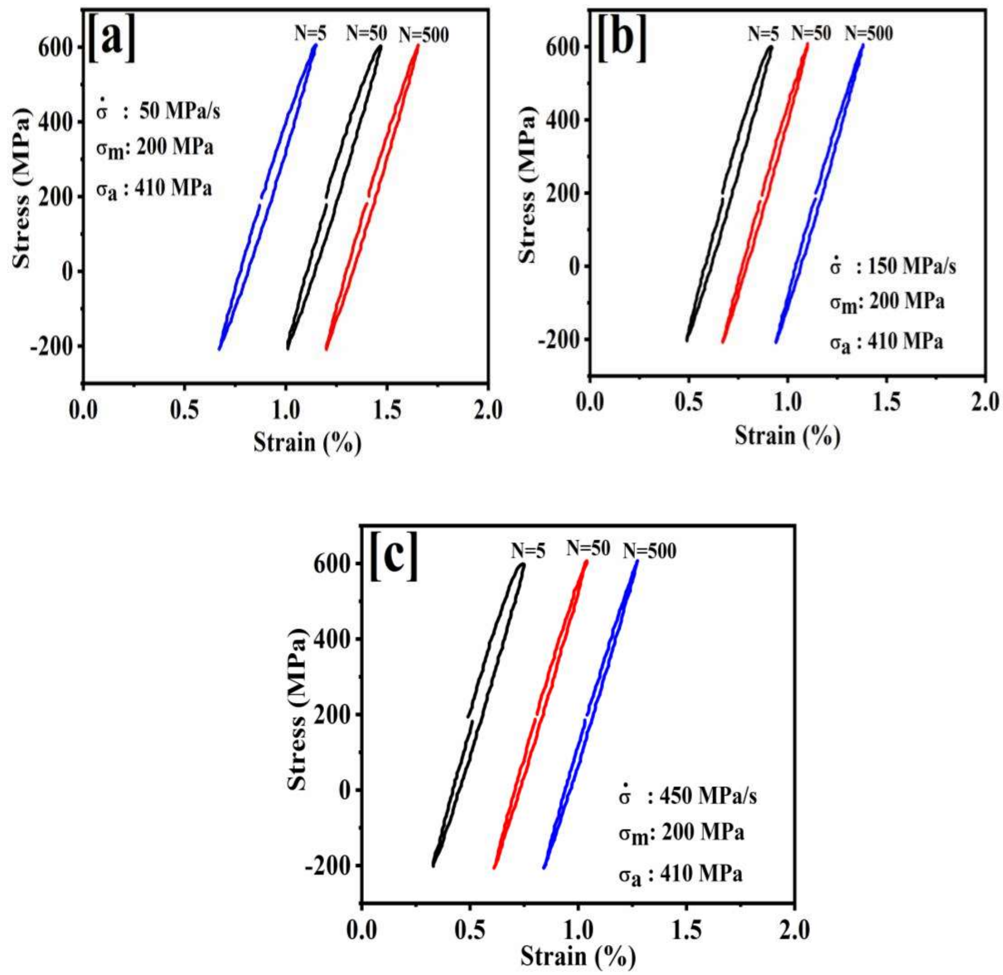

Fig. 3.15 Hysteresis loops of modified 9Cr-1Mo steel corresponding to cycle number 5, 50 and 500, at different stress rates: (a) 50 MPa/s, (b) 150 MPa/s and (c) 450 MPa/s at mean stress of 200 MPa and stress amplitude of 410 MPa.

Fig. 3.16 displays variation in plastic strain energy of loops at different number of cycles, with stress rate. The plastic strain energy is the highest at the lowest stress rate of 50 MPa/s, and it decreases at the higher stress rate of 150 MPa/s and again increases during the later stage (N: 500 cycles). The variation in plastic strain energy of the loops corresponding to 50th and 500th loops shows continuous decrease in plastic strain energy with increase in stress rate from 50 MPa/s to 450 MPa/s. Thus, with increase in stress rate, the absorbed plastic strain energy decreased and cyclic hardening of the material was observed.

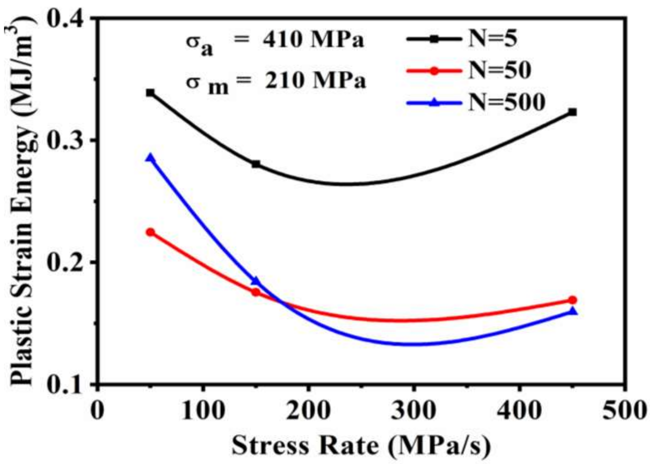

Fig. 3.16 Effect of stress rate on hysteresis loop energy of modified 9Cr-1Mo steel, at different number of cycles at constant mean stress of 200 MPa and stress rate of 150 MPa/s.

3.6 Influence of asymmetric stress cycling on fracture behaviour of modified 9Cr-1Mo steel

Fracture behaviour of all the samples tested at room temperature, in different combinations of the variables such as mean stress, stress amplitude and stress rate was characterized by SEM. Since the loading was asymmetric and a tensile mean stress was acting on the specimen continuously, the specimens failed in ductile manner exhibiting cup and cone type fracture.

Examination of the specimens fractured from ratcheting fatigue revealed two distinct regions; one of light contrast and annular shape, and the other of darker contrast and flat shape, in the central region. While the annular region shows tapering, the central region is flat (Fig. 3.17a). Since there was progressive necking in the specimen, the fractured piece, up to a specified length from the fractured end appeared like frustum of a conical shape. The examination of the annular region at higher magnification revealed features like fatigue striations (Fig. 3.17b) whereas the central flat region depicts dimples (Fig. 3.17c). Fig. 3.17(d) clearly shows both the regions; the one on the left side shows striations and that on the right side exhibits dimples; thus, the demarcation between the two regions of distinct morphology is quite evident.

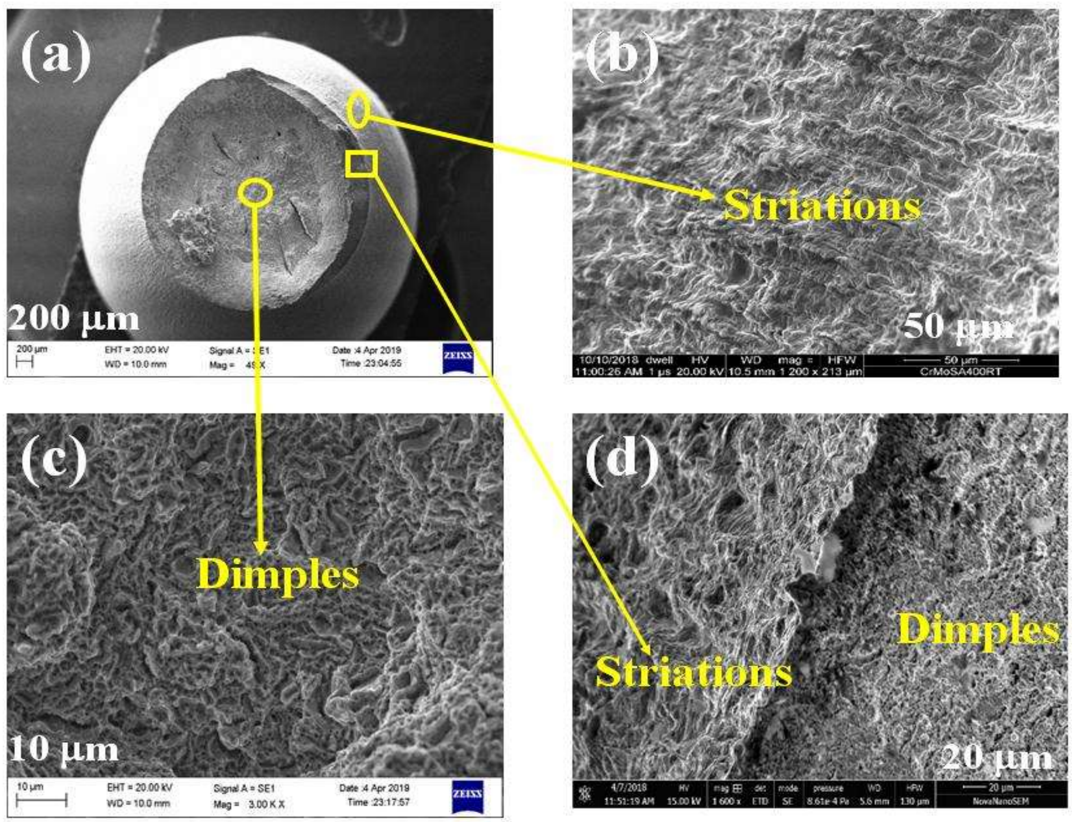

Fig. 3.17 SEM fractographs of modified 9Cr-1Mo steel fatigue sample tested, under asymmetrical cyclic loading at stress amplitude of 400 MPa , mean stress of 200 MPa and stress rate of 150 MPa/s: (a) full view of the fracture end with flat fracture surface and tapered annular region (b) magnified view of the surface from the annular region showing features like striations (c) magnified view of the flat transverse fracture surface showing dimples and (d) magnified view of the junction of the annular region showing striations in the annular region on left side and dimples on the flat surface on the right side.

Fig. 3.18(a) shows photograph of the fatigue specimen fractured due to asymmetric cyclic stressing. The necked region in the centre may clearly be seen. For better understanding, a schematic representation of the fractured specimen is displayed in Fig. 3.18(b) in vertical orientation of the fracture end (top view), displaying a flat region in the centre and the annular region with feature like striations. The isometric view in Fig. 3.18(c) presents the flat fracture end with dimples in the central region and tapered length of the frustum of the cone-like shape in the necked region with striation like features.

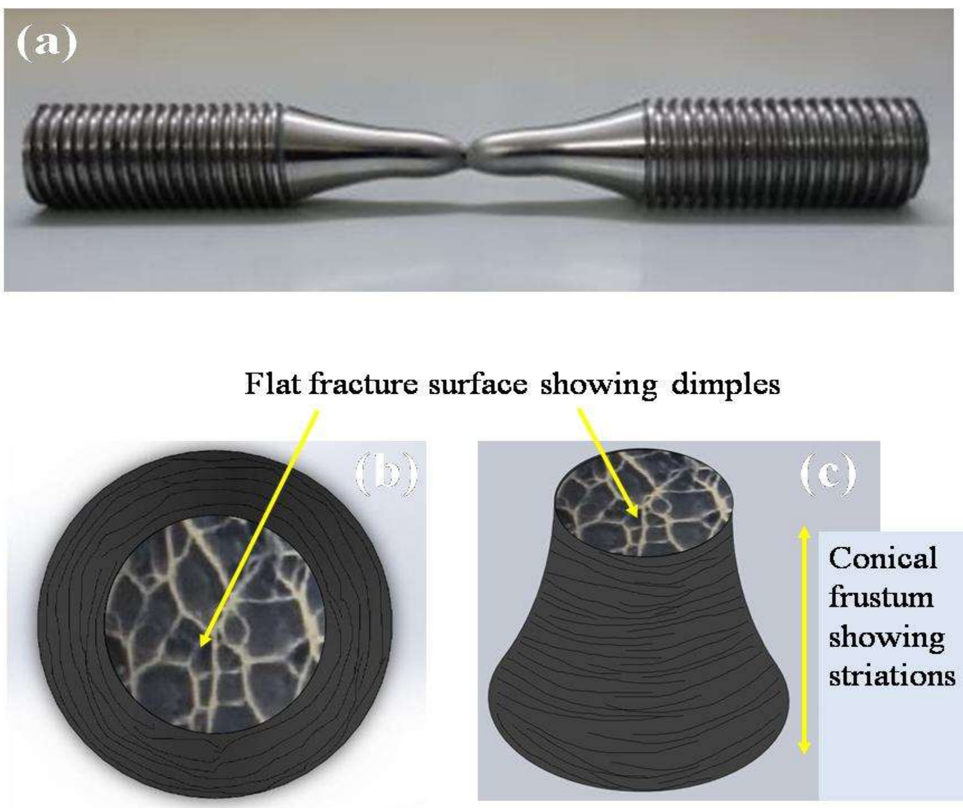

Fig. 3.18 Features of modified 9Cr-1Mo steel fatigue specimen fractured under ratcheting fatigue: (a) fatigue specimen fractured from ratcheting fatigue showing necking (b) schematic presentation of the fracture end in vertical orientation showing flat surface in the central region with dimples and annular region showing striation like features and (c) isometric view of the fracture end showing flat fracture surface at the top with dimples and tapered surface of cone like frustum with striations.

Fractographic studies of the modified 9Cr-1Mo steel fatigue fracture have been carried out by several researchers but this type of fracture, resulting from asymmetric cyclic loading (ratcheting), has not been reported yet. The cause of this type of typical failure is the tensile mean stress acting constantly on the specimen. Fatigue cracks initiate from the surface but they do not propagate transversely like that under symmetrical cyclic loading, rather propagate axially due to continuous action of the tensile mean stress. The progressive axial accumulating plastic strain in specimen length led to increase in length of specimen and caused necking, and led to the ultimate failure in tensile mode, exhibiting distinct dimples.

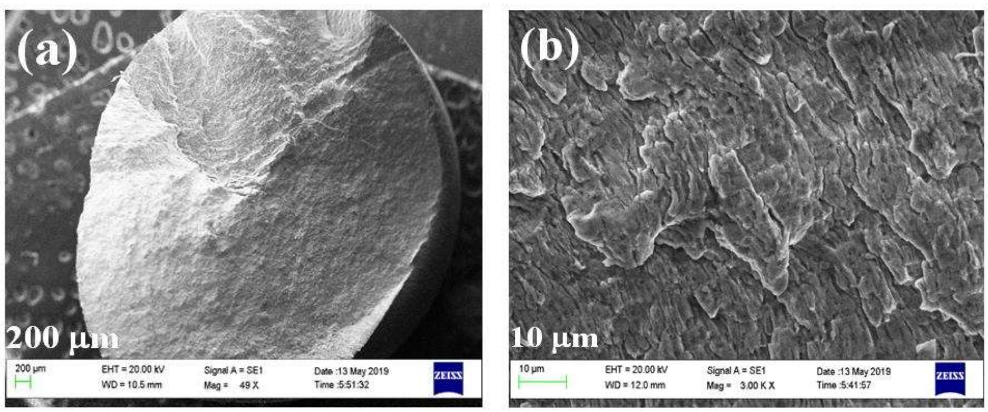

Fig. 3.19 SEM fractographs of modified 9Cr-1Mo steel fatigue sample, tested under symmetrical cyclic loading (without mean stress) at stress amplitude of 510 MPa and stress rate of 150 MPa/s showing: (a) absence of annular region and (b) magnified view of the fracture surface showing striations on the fracture surface in the region of fatigue crack propagation.

For comparison, a stress-controlled fatigue test was conducted under symmetrical loading (without mean stress), till failure at the stress amplitude of 510 MPa and its fracture surface was examined under SEM. It was found that there was no necking and no annular circumferential feature (Fig. 3.19a). The usual fatigue striations resulting from fatigue crack propagation was observed on the fracture surface (Fig. 3.19b).These observations are similar to that observed by Verma et al., (2016) under symmetric strain-controlled cyclic loading of the modified 9Cr-1Mo steel at room temperature.

Thus, the variation in fracture surfaces is due to difference in the kind of loading, (symmetrical /asymmetrical). In the case of asymmetric cyclic loading, there is simultaneous action of the tensile mean stress on the test specimen, to give rise to the observed fracture behaviour. Ductile cup and cone fracture is related to asymmetric loading, depending upon the magnitude of the accumulated plastic strain resulting from the asymmetric cyclic loading and the uniform plastic strain of the material. In the case of modified 9Cr-1Mo steel, cup and cone type fracture occurred during asymmetric cyclic loading, because its uniform plastic strain was less than the accumulated plastic strain, resulting from ratcheting; hence, necking occurred. When the diameter of the specimen in the necked region got reduced drastically and true stress increased the fracture strength, fracture occurred in tensile mode exhibiting cup and cone features.

3.7 Deformation behaviour of modified 9Cr-1Mo steel

The deformation behaviour of the modified 9Cr-1Mo steel under asymmetrical stress-controlled cyclic loading is associated with dynamic recovery. The tempered lath martensite with a high density of dislocations in the as-received condition (Fig. 3.2a and b) exhibited instability under cyclic loading and transformed to equiaxed substructure of large size. The observed cyclic softening due to rise in mean stress / stress amplitude and reduction in stress rate may be essentially from the development of cell structure and dynamic recovery.

The process of deformation and recovery can be very well explained with the help of TEM micrographs from the following three conditions of ratcheting fatigue.

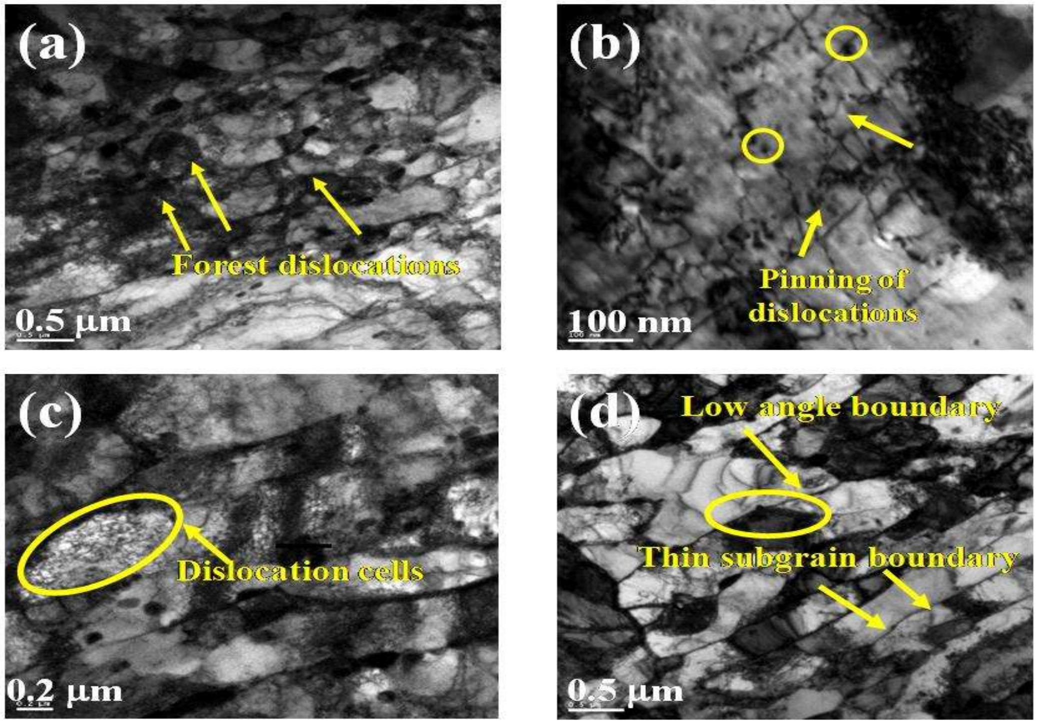

Fig. 3.20 Bright field TEM micrographs showing stages of deformation in the modified 9Cr-1Mo steel in different loading conditions of stress amplitude, mean stress and stress rate at RT under asymmetrical cyclic loading showing: (a) forest dislocations (stress amplitude of 400 MPa , mean stress of 200 MPa, stress rate of 150 MPa/s) (b) pinning of dislocations by very fine carbide precipitates shown by circles and arrows (stress amplitude of 400 MPa , mean stress of 200 MPa, stress rate of 150 MPa/s) (c) dislocation cells (stress amplitude of 410 MPa , mean stress of 200 MPa, stress rate of 150 MPa/s and (d) recovered subgrain structure (stress amplitude of 400 MPa, mean stress of 210 MPa, stress rate of 150 MPa/s).

Stage I- Fig. 3.20(a) shows high density of forest dislocations, those do not cancel under tension–compression cycles because of their different orientations; Fig. 3.20(b) displays pinning of dislocations by carbide particles. Both of these phenomena caused hardening of the material at the lowest mean stress / stress amplitude and at higher stress rate.

Stage II-Fig. 3.20(c) shows formation of dislocation cells, a clear indication of softening in the material at the intermediate mean stress / stress amplitude and stress rate.

Stage III- Fig. 3.20(d) shows well-defined boundaries with almost equiaxed substructure which confirms that recovery has taken place and caused softening of the material at higher mean stress / stress amplitude and lower stress rate.

Verma et al., (2016) investigated high strain fatigue behaviour of the modified 9Cr-1Mo steel at RT and found that cyclic softening occurred, irrespective of the strain amplitude and strain rate, and only dislocation cells were observed under symmetrical strain-controlled cycling.

3.8 DISCUSSION

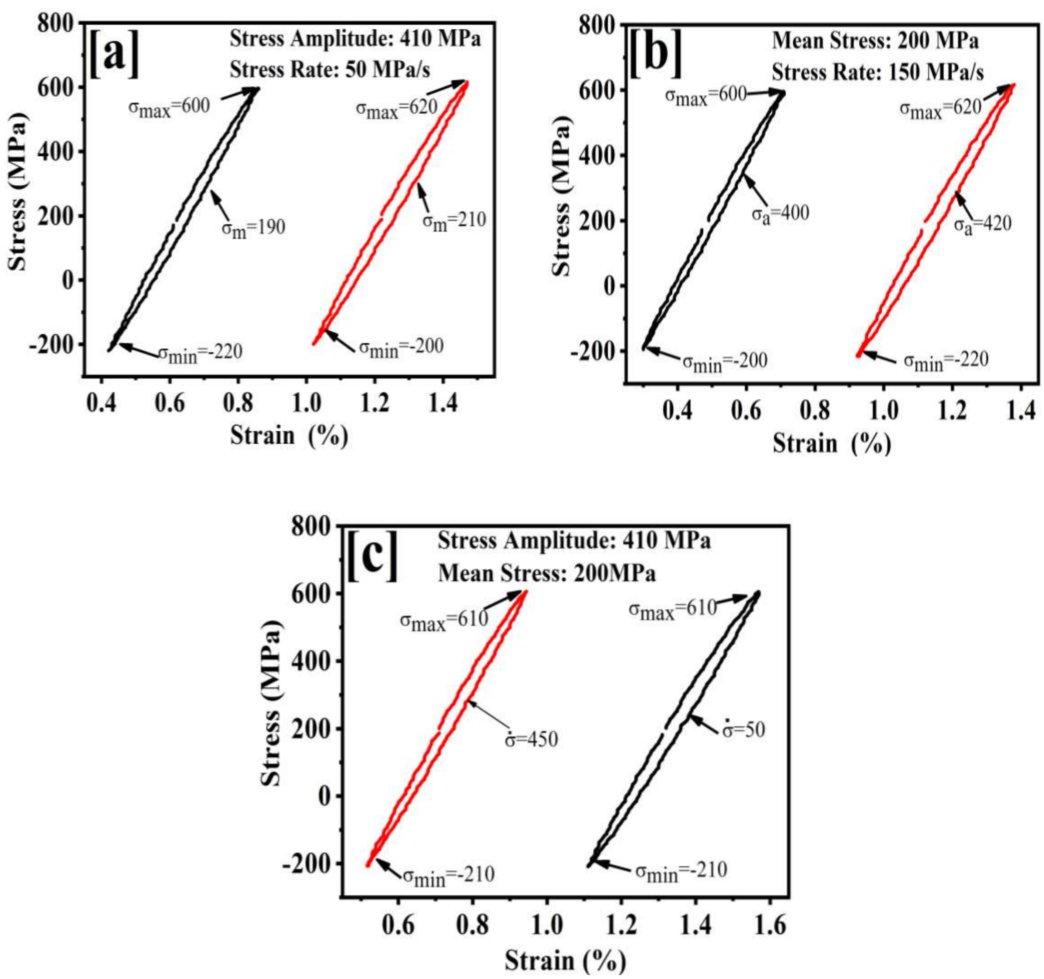

Fig. 3.21 Shifting of 20th cycle loop towards tensile direction of modified 9Cr-1Mo steel, due to increase in (a) mean stress from 190 MPa to 210 MPa (b) stress amplitude from 400 MPa to 420 MPa and (c) stress rate from 50 MPa/s to 450 MPa/s.

The hysteresis loops of the 20th cycle at mean stress of 190, 200 and 210 MPa were recorded to examine the impact of tensile mean stress on the accumulation of plastic strain in asymmetric cyclic loading, at RT. The loops of the 20th cycle for mean stress of 190 MPa and 210 MPa are presented in Fig. 3.21(a)

The degree of non-closure of the loops increased with increase in mean stress from 190 to 210 MPa, because of higher accumulation of plastic strain, consistent with the earlier observations [Rajpurohit et al., (2018)]. It was further noted that at higher mean stress, the hysteresis loop shifted to the tension side showing larger damage accumulation and loss of fatigue life. The increase in the level of the hysteresis loop of the 20th cycle for mean stress of 210 MPa is due to increase in the magnitude of mean stress. The width of the hysteresis loop of the 20th cycle increased from the rise of mean stress, which is due higher extent of plastic deformation. Further, the plot of plastic strain energy shows that plastic strain energy increased with rise of mean stress, because of higher plastic deformation (Fig. 3.22).

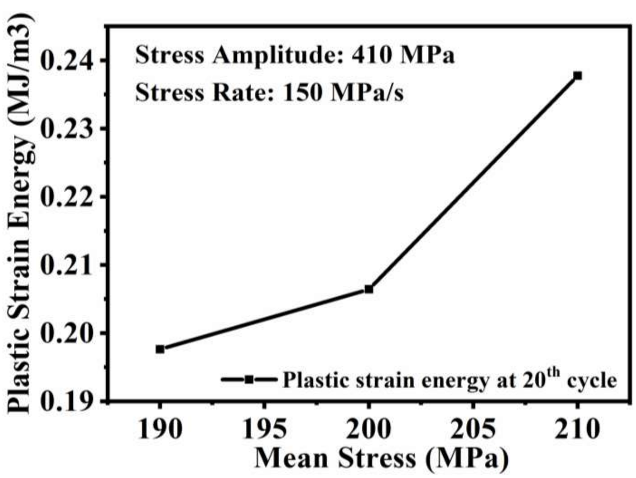

Fig. 3.22 Dependence of plastic strain energy on mean stress of modified 9Cr-1Mo steel corresponding to 20th cycle at stress amplitude of 410 MPa and stress rate of 150 MPa/s.

From the rise in the tensile mean stress, ratcheting strain accumulation and also its rate increased rapidly. This behaviour is in agreement with Cheng et al., (2015) in which the rise in mean stress led to a decrease in fatigue life of the specimen because of increase in the accumulated ratcheting strain. TEM micrographs of the specimens tested at mean stress of 190 MPa and 210 MPa displaying dislocation cells and substructure are shown in Fig. 3.23.

At the lower mean stress of 190 MPa, all the dislocations have not annihilated to give rise to substructure. Dislocations are rearranged as cells. Dislocation cell walls are shown in Fig. 3.23 which indicates incomplete conversion to substructure (incomplete recovery). However, at higher mean stress of 210 MPa, thinner cell walls are seen, and grain boundaries are sharp (low angle boundaries) which define substructure as shown in Fig. 3.20(d). Sharpness of cell boundaries increases with increase in the mean stress. The dislocation cell structure and size varied with mean stress. Dislocation cell formation is responsible for softening. It is a stage prior to formation of a substructure. With the rise in mean stress from 190 MPa to 210 MPa, recovery has taken place which is manifestation of the softening of the material.

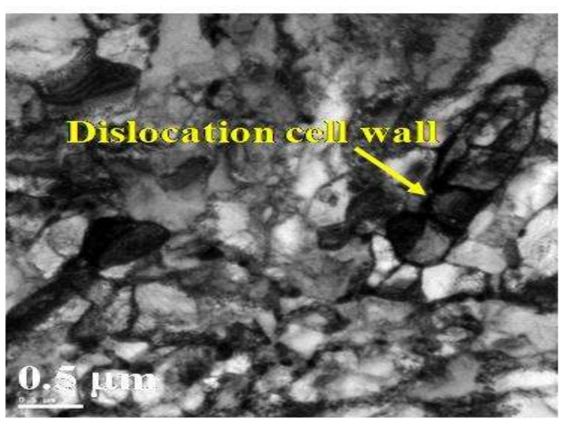

Fig. 3.23 Bright field TEM micrograph of modified 9Cr-1Mo steel fatigue sample, tested at mean stress of 190 MPa, stress amplitude of 400 MPa and stress rate of 150 MPa/s, showing dislocation cell walls (incomplete recovery).

With the aid of microscopy of the fatigue sample interrupted at 2205 cycles, screw dislocations are observed in the form of jogs, formed due to intersection of dislocations and some extended dislocations are also seen (Fig. 3.24); this is a clear sign of hardening of the material.

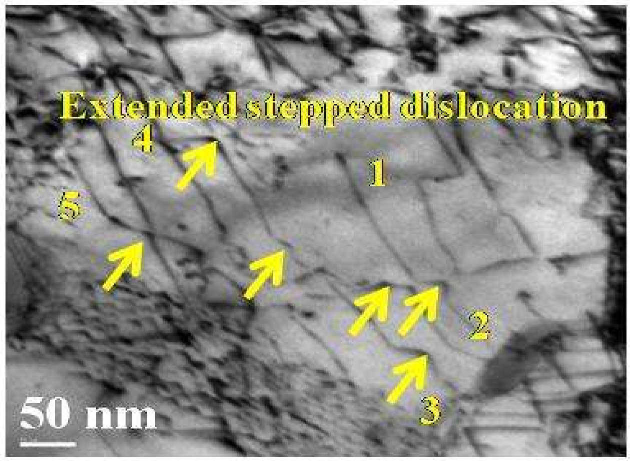

Fig. 3.24 Bright field TEM micrograph of modified 9Cr-1Mo steel fatigue sample, interrupted at 2205 cycles, tested at stress amplitude of 410 MPa, mean stress of 200 MPa, and stress rate of 150 MPa/s, showing extended stepped dislocation (jogs).

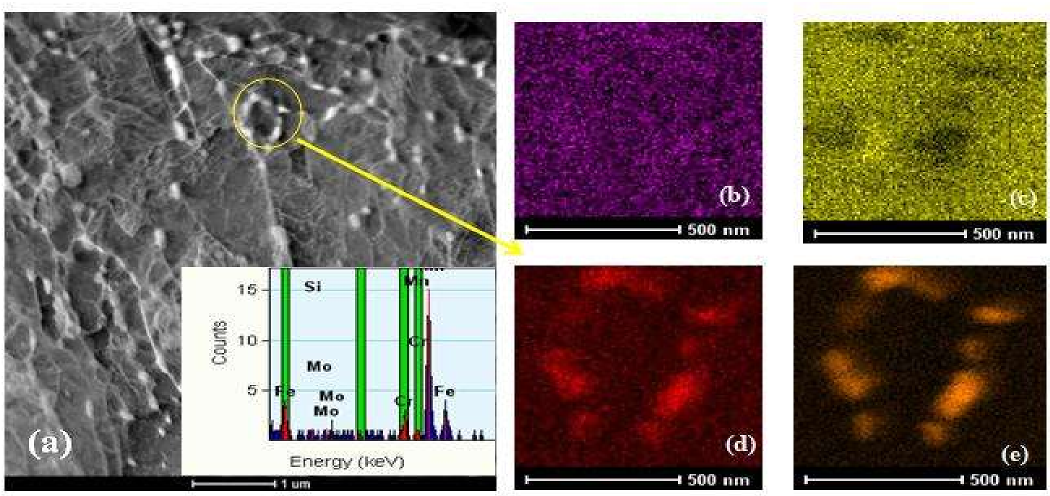

Fig. 3.25 STEM micrograph and EDX analysis of of modified 9Cr-1Mo steel fatigue sample, interrupted at 2205 cycles, tested at stress amplitude of 410 MPa, mean stress of 200 MPa, and stress rate of 150 MPa/s, showing: (a) region of mapping (b) matrix (c) Cr (d) Fe and (e) V.

Fig. 3.25(a) shows micrograph using scanning transmission electron microscope (STEM) and Energy dispersive X-Ray spectroscopy (EDX) of the specimen interrupted at 2205 cycles and Figs. 3.25(b, c, d and e) shows elemental mapping, which indicates no new phase formation. From the SEM fractographs, fatigue signatures (striation like features) may be observed on the outer peripheral surface (Fig. 3.18b) and the flat transverse fracture surface shows typical ductile fracture with distinct dimples, resulting from tensile mean stress, acting on the specimen. Therefore, the reason behind the decrease in fatigue life due to the increase in mean stress was essentially due to increase in accumulated plastic strain.

With the rise in stress amplitude from 400 to 420 MPa, cyclic life was drastically reduced as observed from Table 3.3. The accumulated ratcheting strain significantly increased with rise in stress amplitude and hence it is evident that the effect of stress amplitude on fatigue life was significantly higher than the effects of mean stress and stress rate. Hysteresis loops of the 20^{th} cycle of the samples tested at varying stress amplitude of 400 to 420 MPa, at mean stress of 200 MPa and stress rate of 150 MPa/s are shown in Fig. 3.21(b).

Similar behaviour was noticed also in the case of stress amplitudes as in the case of the mean stress. Cyclic life decreased from the rise in stress amplitude due to increase in accumulation of ratcheting strain (Fig. 3.6a), in line with earlier observations [Lin et al., (2013); Kreethi et al., (2017)]. It was also seen that, with rise in stress amplitude from 400 MPa to 420 MPa, there was difference in the size and shape of the hysteresis loops, as shown in Fig. 3.21(b).

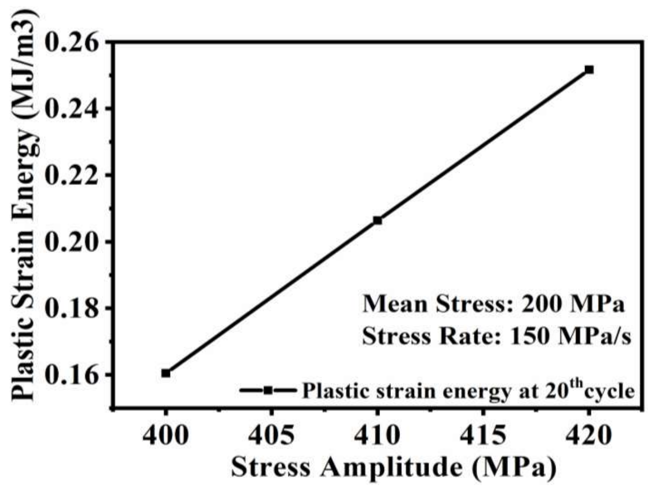

Fig. 3.26 Dependence of plastic strain energy on stress amplitude of modified 9Cr-1Mo steel, corresponding to 20^{th} cycle at mean stress of 200 MPa and stress rate of 150 MPa/s.

There was continuous increase in the plastic strain energy from the increase in stress amplitude exhibiting higher plastic deformation of the material (Fig. 3.26). Thus, the rise in stress amplitude from 400 to 420 MPa, resulted in decrease in the cyclic life which was essentially due to increase in accumulated plastic strain.

The TEM micrographs of the specimens tested at the lower stress amplitude of 400 MPa did not show fully recovered cells whereas elongated structure was observed which is essentially due to lath structure of martensite (Fig. 3.27a). High density of forest dislocations along with very fine carbide precipitates and pinning of the dislocations was observed (Figs. 3.20a and b) which led to hardening of the material. Regions of cell formation are identified in the intermediate range of stress amplitude and mean stress of 410 MPa and 200 MPa, respectively (Fig. 3.20c).

On the other hand, at higher stress amplitude of 420 MPa fully recovered structure with sharp boundaries was observed (Fig. 3.20d), showing clear indication of dynamic recovery and the cause for decrease in cyclic life of the material. The structure at highest stress amplitude of 420 MPa was found to be equiaxed in shape (Fig. 3.27b). The SEM fractrographs showed a similar ductile fracture as already discussed in case of the mean stress effect but also showed fatigue signatures to a certain extent (Fig. 3.18b) which is basically due to the type of loading. Fig. 3.27(c) shows TEM micrograph of the sample tested in fatigue at 400 MPa and its corresponding diffraction pattern (Fig. 3.27d) including the matrix (*bcc*) and $Cr_{23}C_6$ precipitate (*fcc*).

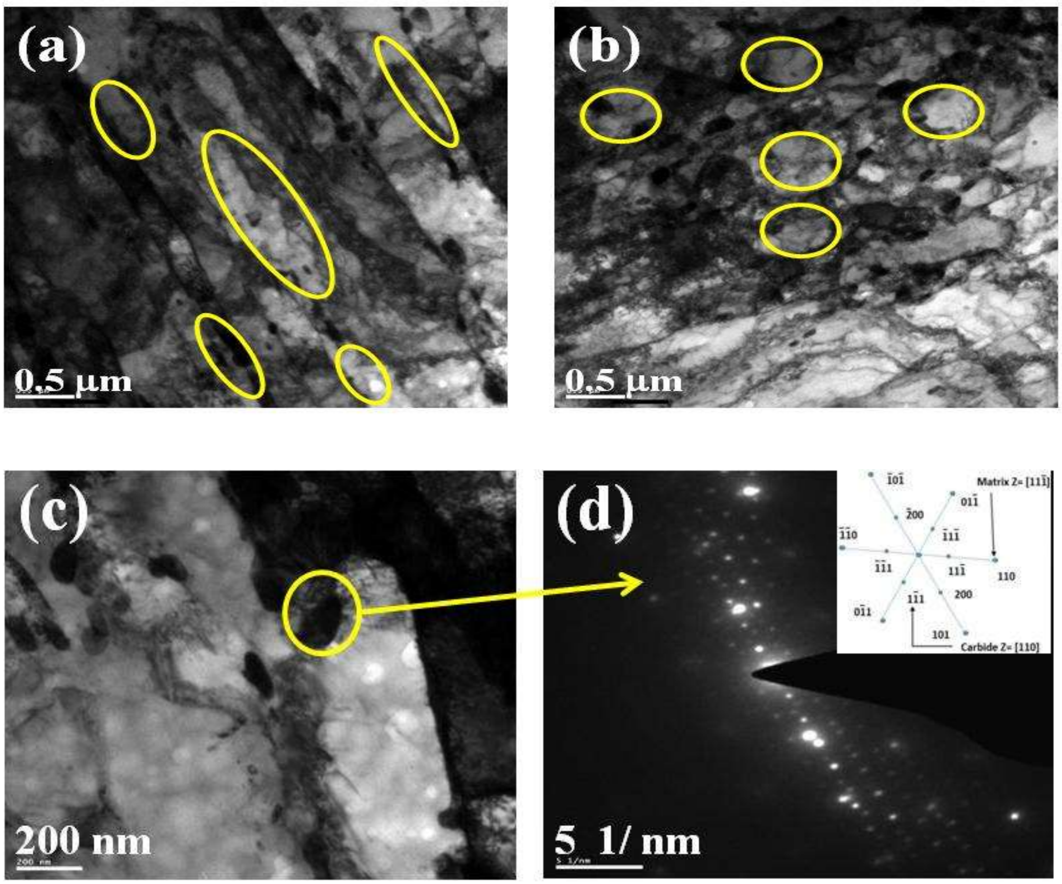

Fig. 3.27 TEM micrographs of of modified 9Cr-1Mo steel fatigue sample, tested at different stress amplitudes showing: (a) elongated lath structure at stress amplitude of 400 MPa, mean stress of 200 MPa and stress rate of 150 MPa/s (b) equiaxed structure at stress amplitude of 420 MPa, mean stress of 200 MPa and stress rate of 150 MPa/s (c) matrix and precipitates at stress amplitude of 400 MPa, mean stress of 200 MPa and stress rate of 150 MPa/s and (d) diffraction pattern of the matrix and prcipitate ($Cr_{23}C_6$).

The influence of stress rate on the cyclic stress-strain hysteresis loops is presented in Fig. 3.21(c). It may be seen that with the rise in stress rate, there is a decrement in the width of the hysteresis loops exhibiting hardening behaviour. Due to rise in stress rate from 50 MPa/s to 150 MPa/s plastic strain energy for 20^{th}cycle decreased, but slight increase was observed in the plastic strain energy with increase in stress rate from 150 MPa/s to 450 MPa/s (Fig. 3.28a). After critical examination it was observed that in 50^{th}, $500^{th}$and 1000^{th} cycle, the plastic strain energy continuously decreased with increase in stress rate (Fig. 3.28b). However, the overall plastic strain energy for the 20^{th} cycle decreased from the rise in stress rate from 50 MPa/s to 450 MPa/s (Fig. 3.28). Due to rise in the stress rate, cyclic frequency increases which hinders the movement of dislocations and results in increased fatigue life.

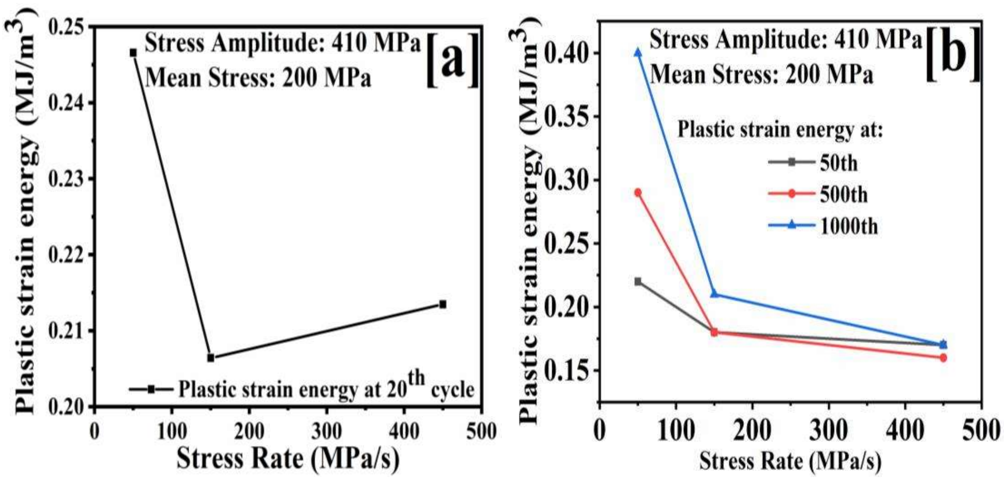

Fig. 3.28 Dependence of plastic strain energy on stress rate of modified 9Cr-1Mo steel, corresponding to: (a) 20^{th} cycle (b) 50^{th}, 500^{th} and 1000^{th} cycle at mean stress of 200 MPa and stress amplitude of 410 MPa.

TEM micrograph of the fatigue tested sample at lower stress rate of 50 MPa/s shows recovered structure with distinct boundaries (Fig. 3.29a). On the other hand, at the higher stress rate of 450 MPa/s, formation of dislocation cells along with dense forest dislocations takes place (Fig. 3.29b) which leads to hardening and consequent increase in cyclic life. The fracture behaviour was similar to that discussed for the effect of mean stress and stress amplitude.

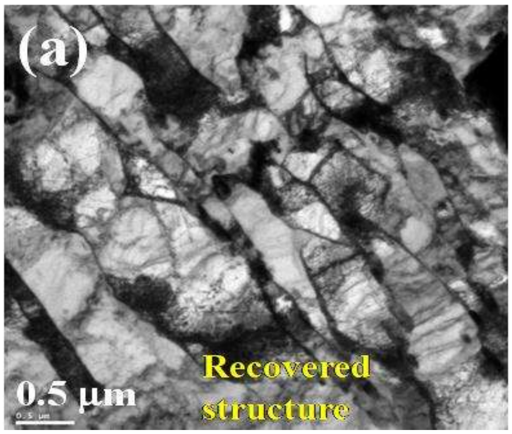

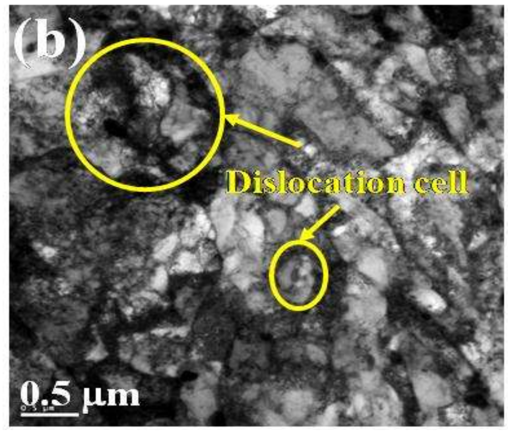

Fig. 3.29 Bright field TEM micrographs of modified 9Cr-1Mo steel fatigue sample, tested at different stress rates showing: (a) recovered structure at stress rate of 50 MPa/s, stress amplitude of 410 MPa and mean stress of 200 MPa (b) formation of dislocation cells along with dense forest dislocations at stress rate of 450 MPa/s, stress amplitude of 410 MPa and mean stress of 200 MPa.

3.9. Summary

The important inferences that can be drawn from this study on the ratcheting fatigue behaviour of modified 9Cr-1 Mo steel at room temperature are listed below.

1. There was accumulation of plastic strain under asymmetric cyclic loading. The accumulated plastic strain was tensile in nature and increased with increase in mean stress and stress amplitude and consequently, fatigue life was reduced, whereas the accumulation of plastic strain was reduced with increase in stress rate and fatigue life was increased.
2. With increase in the mean stress from 190 to 210 MPa and stress amplitude from 400 to 420 MPa, the width of hysteresis loops increased and plastic strain energy

also increased due to higher plastic deformation of the material. On the other hand, with increase in number of cycles the material exhibited cyclic hardening, for a particular value of a parameter.

3. With increase in stress rate, the plastic strain energy as well as hysteresis loop width decreased, due to higher cyclic work hardening of the material. This resulted from combined effects of higher density of dislocations produced at higher stress rate and less effective annihilation of dislocations, during the tensile and compressive load cycles. Thus, the overall density of dislocations was higher at higher stress rate, due to which the work hardening increased with increase in stress rate. The extent of hardening increased with number of cycles at all the three stress rates of 50, 150 and 450 MPa/s. The decrease in the ratcheting strain in consecutive cycles was due to the increase in rate of hardening.
4. Under symmetrical loading, there was characteristic fatigue fracture with typical striations on the fracture surface resulting from crack propagation from surface to interior, finally leading to overload ductile failure with dimples. However, under asymmetrical loading, there was increase in gauge length and appreciable necking before fracture. There were striations like features on the surface of tapered necked region resulting from cyclic plastic flow on the tapered surface and the transverse fracture surface was similar to that resulting from tensile loading of ductile material exhibiting characteristic dimples.
5. The observation and understanding of the unique fracture behaviour with striations like features on the smooth circumferential surface in necked region, and ductile tensile cup and cone features with equiaxed dimples on the fracture surface, are interesting aspects of this investigation.

6. There was considerable variation in the deformed microstructures, resulting from different variable such as mean stress, stress amplitude and stress rate. While the laths of martensite were seen in the specimens tested at stress amplitude of 400 MPa, equiaxed structure resulted at stress amplitude of 420 MPa. There was incomplete recovery at mean stress of 190 MPa and formation of recovered substructure at mean stress of 210 MPa. While there was recovered substructure at stress rate of 50 MPa/s, dislocation cells along with forest dislocations were seen at stress rate of 450 MPa/s.